NOLTA, IEICE

Paper

Reduced systems for Intrinsic Localized Modes on an infinite oscillator array

Daniel Brake [1 a)] *and Vakhtang Putkaradze* [2]

[1] *Department of Mathematics, Colorado State University*
101 Weber Building, Fort Collins, Colorado, 80523, USA

[2] *Department of Mathematics, University of Alberta*
CAB 632, Edmonton, AB T6G 2G, Canada

[a)] *brake@math.colostate.edu*

Received October 27, 20XX; Revised December 29, 20XX; Published July 1, 20XX

Abstract: We reduce the complex mechanics of an Intrinsic Localized Mode (ILM) on an infinite monodirectional nonlinear coupled oscillator array. By using Hamiltonian Mechanics, we derive two systems – a simple case when only the position of the ILM is allowed to vary, and the more complex case where both position and amplitude are allowed to change with time. We arrive at a systems of nonlinear equations of motion. For the position-only system, the dynamics are determined solely by the level sets of the Hamiltonian. The four-variable system has a richer structure. We also analyze the effect of a defect, or an impurity, on the motion of the ILM within our framework.

Key Words: Intrinsic Localized Modes, nano resonator, Hamiltonian Mechanics

1. Introduction

The existence of the oscillatory phenomenon called Intrinsic Localized Mode (ILM) has been demonstrated in many coupled systems of oscillators, as early as 1958 [1], and rediscovered in anharmonic pure crystals, as reported in the seminal papers [15, 22]. Since their initial discovery, ILMs have been found in a wide variety of physical and simulated structures, having a variety of nonlinearities; *e.g* linear oscillator lattices with cubic or quartic terms in the Hamiltonian [8]. Many different forms of ILM have been developed and investigated, such as 'twisted un/staggered modes' [11] and 'bright compact breathers' [10]. Scientists have used a plethora of simulated and physical experiments to investigate ILMs, including: micromechanical coupled oscillator arrays [5, 12, 13, 16–19, 21]; biaxial antiferromagnets [20]; 2D coupled oscillator arrays [4]; and coupled arrays of ring oscillators [9]. A more exhaustive historical treatment of the development of ILM can be found in the introduciton to [18].

The nonlinear arrays used for generating ILMs are typically mathematically treated by the Klein-Gordon equations, which are cubic second order ordinary differential equations. A variety of methods are used to deal with these equations, including full numerical simulations [17], and reduced models such as Invariant-Manifold method [5]. Other models have been used to treat nonlinear oscillators, using analytical techniques like multiple-scales method [7].

The goal of this paper is to describe an ILM by low-dimensional dynamics, mimicking deformation of the shape and position of the real ILM. Preliminary investigations performed by this method have been published by the authors in [14]. We shall follow the paradigm of *variational methods* [3] that has been applied to various problems stemming from Hamiltonian mechanics; in particular, we will use the minimal action principle. Starting from what is now the canonical set of equations for a nonlinear oscillator, the Klein-Gordon equations, we will assert a symmetric alternating exponential form for an ILM on an infinite array, and derive simplified equations which characterize the amplitude, velocity, and generalized momenta of the ILM.

This paper is organized as follows. In Section 2, we describe the setup and assumptions for the derivation of the model. Section 3 derives a reduction from an infinite dimensional system to a two-variable system, described by velocity and momentum of the ILM; in parallel fashion, Section 4 derives a model with four variables, as velocity, amplitude, and momenta. The conclusion follows in Section 5.

2. Model

In order to understand ILM dynamics, we derive and simulate a reduced system. Our goal is to derive a consistent, low-dimensional approximation to the dynamics. The order of the reduced system will be proportional to the number of ILMs, rather than the number of oscillators for the full systems. In our derivation, we assume an infinite array of oscillators (as opposed to periodic boundary conditions); one direction of deflection; and no dissipation in the system. The rate of change of the shape and position are assumed to be slow as compared with the frequency of ILM motion. Frequently throughout the literature, dissipation is neglected, see *e.g.* [5, 17]. Moreover, simulations and experiments of over 150 oscillators have been conducted, *e.g.* [17], with ILM amplitude dropoff sufficiently high such that approximation by an infinite array is justified.

A given state of the array is described by a vector of deformations u_n, $n = \ldots, -2, -1, 0, 1, 2 \ldots$, and the corresponding velocities $\dot{u}_n$. We choose the particular form for the ILM as a symmetric alternating exponential; see Fig. 1. The form of this exponential approximates numerically determined ILM shapes, such as those in [5, 12]. More precisely, let us take the form of the ILM (1) to be alternating with n, and centered at the point x, which is not necessarily an integer, having peak amplitude A. Let $n_0(x) = floor(x)$ denote the floor of x. In what follows, we will drop the dependence of n_0 on x in the formulas to keep the expressions as manageable as possible; the dependence $n_0(x)$ is always assumed. Assume further that the ILM has temporal period $2\pi/\omega$, and the "sharpness" of the ILM is described by the exponent λ. The meanings of parameters and variables are summarized in Table I.

$$u_n = A \exp(-\lambda |x(t) - n|)(-1)^n \sin(\omega t) \,. \tag{1}$$

Table I. Symbol Interpretation

Symbol	Interpretation
α_1	Linear restoration
α_2	Linear nearest-neighbor coupling
β_1	Cubic restoration force
β_2	Cubic nearest-neighbor coupling
A	Peak amplitude
x	Center of ILM
u_n	Deflection of oscillator
λ	Sharpness of ILM
ω	Temporal Period
n_0	Oscillator immediately left of x

We use potential and kinetic energies of the array corresponding to a form of the Klein-Gordon equations, given by $\mathcal{P}$ and $\mathcal{K}$; see *e.g.* [15, 22] and following papers.

$$\mathcal{P} = \sum_{n=-\infty}^{\infty} \frac{1}{2}(\alpha_1 u_n^2 + \alpha_2(u_n - u_{n-1})^2) + \frac{1}{4}(\beta_1 u_n^4 + \beta_2(u_n - u_{n-1})^4)\,, \tag{2}$$

$$\mathcal{K} = \frac{1}{2}\sum_{n=-\infty}^{\infty} \dot{u}_n^2\,. \tag{3}$$

The system is Hamiltonian, with $\mathcal{H} = \mathcal{K} + \mathcal{P}$. However, right now we are more interested in describing the Lagrangian approach, where the motion comes from minimizing the action

$$\delta\mathcal{S} = \delta \int \big(\mathcal{K} - \mathcal{P}\big)\mathrm{d}t = 0\,. \tag{4}$$

We will proceed by substituting ILM form (1) into (2,3) and subsequently into the action $S = \int \big(\mathcal{K} - \mathcal{P}\big)\mathrm{d}t$, and derive the reduced action that depends on the few parameters only, namely, on $(x, \dot{x})$ and, eventually, on $(x, \dot{x}, A, \dot{A})$. Low-dimensionality will be achieved by averaging out the quickly oscillating terms.

3. Two Variable Model

In this section, A is taken to be a constant in (1), and only the position x is allowed to vary with time. In Section 4, we will allow both $x(t)$ and $A(t)$ which will lead to substantially more complex equations; the case of x-dependence only is considered as the logical first step.

3.1 Derivation

Kinetic Energy The kinetic energy is computed from the expression (3) by observing that the time derivative $\dot{u}_n$ is given by

$$\dot{u}_n = (-1)^n A \exp(-\lambda|n-x|)\,(-\omega\sin(\omega t) + \lambda\cos(\omega t)\,\mathrm{sign}(n-x)\,\dot{x}) \tag{5}$$

Substitution of (5) into (3) yields,

$$\mathcal{K} = \frac{1}{2}\sum_{n=-\infty}^{\infty} \dot{u}_n^2 = \frac{A^2}{2}\sum_{-\infty}^{n_0} \exp(-2\lambda(x-n))(-\omega\sin\omega t + \lambda\cos(\omega t)(-1)\,\dot{x})^2$$
$$+ \frac{A^2}{2}\sum_{n_0+1}^{\infty} \exp(-2\lambda(n-x))(-\omega\sin\omega t + \lambda\cos(\omega t)\,\dot{x})^2\,.$$

Recognizing the geometric sum,

$$\sum_{n=-\infty}^{m} e^{d\lambda n} = \frac{e^{d\lambda m}}{1-e^{-d\lambda}}\,, \tag{6}$$

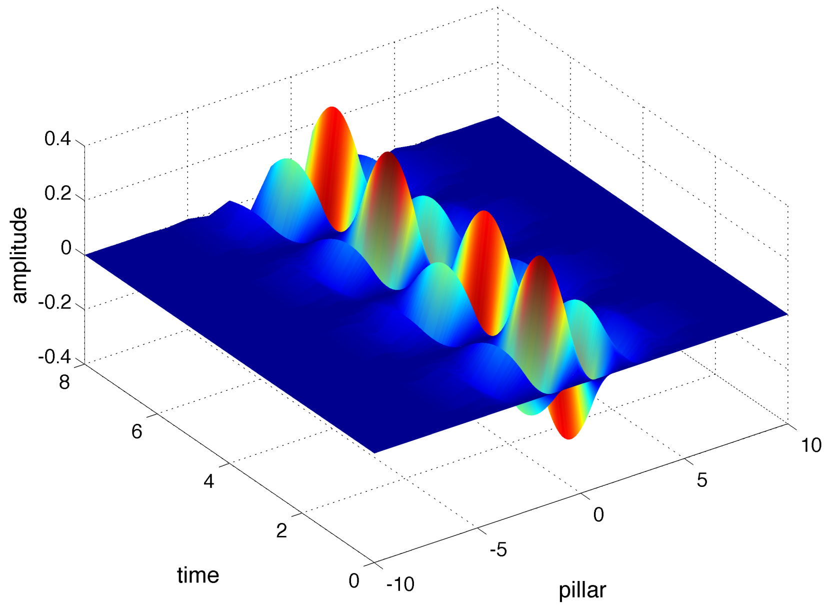

Fig. 1. ILM form. The horizontal axes correspond to the spatial and temporal dimension, the ILM being a decaying alternating exponential spatially, and periodic temporally. The center of the ILM is not necessarily an integer, and the peak may lie between oscillators.

we then get,

$$\begin{aligned}\mathcal{K} = &\frac{A^2}{2}\left(\omega^2\sin^2\omega t + 2\omega\lambda\sin\omega t\cos\omega t + \lambda^2\cos^2\omega t\,\dot{x}^2\right)\frac{\exp(-2\lambda(x-n_0))}{1-\exp(-2\lambda)}\\ &+\frac{A^2}{2}\left(\omega^2\sin^2\omega t - 2\omega\lambda\sin\omega t\cos\omega t + \lambda^2\cos^2\omega t\,\dot{x}^2\right)\frac{\exp(-2\lambda(n_0+1-x))}{1-\exp(-2\lambda)}\,.\end{aligned}$$

Computing the long-term integral in the action and dividing, for convenience, by the length of the time interval, we see that the expressions involving each of $\sin^2\omega t$, $\cos^2\omega t$, and $\sin\omega t\cos\omega t$ are averaged over one period of oscillation as follows:

$$\begin{aligned}\frac{1}{T}\int_0^T \sin^2\omega t\,\mathrm{d}t \to \frac{1}{2}\,, &\quad T\to\infty\,,\\ \frac{1}{T}\int_0^T \cos^2\omega t\,\mathrm{d}t \to \frac{1}{2}\,, &\quad T\to\infty\,,\\ \frac{1}{T}\int_0^T \sin\omega t\cos\omega t\,\mathrm{d}t \to 0\,, &\quad T\to\infty\,.\end{aligned}$$

Therefore, we get the averaged kinetic energy $\mathbb{K}$

$$\mathbb{K} := \frac{1}{T}\int_0^T \mathcal{K}\mathrm{d}t \to \frac{A^2}{2}\frac{\omega + \frac{\lambda^2\pi}{\omega}\dot{x}^2}{1-e^{-2\lambda}}\left(e^{-2\lambda(x-n_0)} + e^{-2\lambda(n_0+1-x)}\right) := \dot{x}^2\,\frac{\psi(x)}{2}\,. \qquad (7)$$

Potential Energy We derive the equations for the potential energy in similar fashion. First we will substitute the ILM form (1) into (2), and then simplify the equations.

$$\mathcal{P} = \frac{1}{2}\left(\alpha_1\mathcal{U}_1 + \alpha_2\mathcal{U}_2\right) + \frac{1}{4}\left(\beta_1\mathcal{U}_3 + \beta_2\mathcal{U}_4\right) \,, \tag{8}$$

$$\mathcal{U}_1 = \sum_{-\infty}^{\infty} u_n^2 \,, \quad \mathcal{U}_2 = \sum_{-\infty}^{\infty}(u_n - u_{n-1})^2 \,, \tag{9}$$

$$\mathcal{U}_3 = \sum_{-\infty}^{\infty} u_n^4 \,, \quad \mathcal{U}_4 = \sum_{-\infty}^{\infty}(u_n - u_{n-1})^4 \,.$$

Again, geometric sums appearing as in (6) may be simplified. Defining the corresponding averages

$$U_i = \lim_{T\to\infty}\frac{1}{T}\int \mathcal{U}_1 \mathrm{d}t, , \quad i = 1, \ldots, 4$$

we get

$$U_1 = \sum_{-\infty}^{\infty} u_n^2 = A^2\cos^2\omega t \sum_{-\infty}^{\infty}\exp(-2\lambda|n-x|) = \frac{A^2}{2(1-e^{-2\lambda})}\left(e^{-2\lambda(x-n_0)} + e^{-2\lambda(n_0+1-x)}\right) \,. \tag{10}$$

$$U_2 = \sum_{-\infty}^{\infty}(u_n - u_{n-1})^2 = A^2\cos^2\omega t \sum_{-\infty}^{\infty}\left(\exp(-2\lambda|n-x|) - \exp(-2\lambda|n-1-x|)\right)^2 \,,$$

$$= A^2\left(\frac{e^{-2\lambda(x-n_0)} + e^{-2\lambda(n_0+1-x)}}{1-e^{-2\lambda}} - e^{-\lambda}\frac{e^{-2\lambda(x-n_0)} + e^{-2\lambda(n_0+2-x)}}{1-e^{-2\lambda}} - e^{-\lambda}\right) \,. \tag{11}$$

The equation for U_3 is derived by direct analogy to the equation U_1 (10):

$$U_3 = \sum_{-\infty}^{\infty} u_n^4 = \frac{A^4\cos^4(\omega t)}{1-e^{-4\lambda}}\left(e^{-4\lambda(x-n_0)} + e^{-4\lambda(n_0+1-x)}\right) \tag{12}$$

$$= \frac{3A^4}{8(1-e^{-4\lambda})}\left(e^{-4\lambda(x-n_0)} + e^{-4\lambda(n_0+1-x)}\right) \,. \tag{13}$$

Finally, the calculation of U_4 is similar to that of U_2 (11), except that there are a few extra multiplicative factors and additive terms.

$$U_4 = \sum_{-\infty}^{\infty}(u_n - u_{n-1})^4 \,, \tag{14}$$

$$= \frac{3A^4}{8}\left(2\frac{e^{-4\lambda(x-n_0)} + e^{-4\lambda(n_0+1-x)}}{1-e^{-4\lambda}} - 4\sigma_a + 6\sigma_b - 4\sigma_c\right) \,, \tag{15}$$

where the σ terms are,

$$\sigma_a = e^{-\lambda}\frac{e^{-4\lambda(x-n_0)}}{1-e^{-4\lambda}} + e^{\lambda}\frac{e^{-4\lambda(n_0+2-x)}}{1-e^{-4\lambda}} + e^{-\lambda}e^{-2\lambda(n_0+1-x)} \,, \tag{16}$$

$$\sigma_b = e^{-2\lambda}\frac{e^{-4\lambda(x-n_0)}}{1-e^{-4\lambda}} + e^{2\lambda}\frac{e^{-4\lambda(n_0+2-x)}}{1-e^{-4\lambda}} + e^{-2\lambda} \,, \tag{17}$$

$$\sigma_c = e^{-3\lambda}\frac{e^{-4\lambda(x-n_0)}}{1-e^{-4\lambda}} + e^{3\lambda}\frac{e^{-4\lambda(n_0+2-x)}}{1-e^{-4\lambda}} + e^{-3\lambda}e^{2\lambda(n_0+1-x)} \,. \tag{18}$$

Finally, we pull out A from each of the U_i, merge the remnants of the U_i into appropriate μ_2, μ_4 and combine them into the new time-averaged potential energy $\mathbb{P}$:

$$\mathbb{P} = A^2\mu_2 + A^4\mu_4 \,. \tag{19}$$

Defect A defect in the array of pillars, introduced to mimic molecule attachment to a nano scale crystal array, can be introduced into this system easily. For demonstration, we defect parameter α_1.

Suppose the defect occurs on pillar k_0, so that *at pillar* k_0, $\tilde{\alpha}_1 = \alpha_1 + \alpha_D$; then we simply have an additive term to $\mathbb{P}$. Therefore, in the presence of a defect,

$$D = \frac{A^2}{2}\alpha_D e^{-2\lambda|x-k_0|}\,, \tag{20}$$

and we can redefine,

$$\mathbb{P} \to \mathbb{P} + D\,. \tag{21}$$

Hamiltonian Mechanics Next, we write the Lagrangian $\mathcal{L}$ for the simplified two dimensional system:

$$\mathcal{L} = \mathbb{K} - \mathbb{P}\,, = \psi(x)\,\frac{\dot{x}^2}{2} - \mathbb{P}\,. \tag{22}$$

Then we define the canonical variable, or generalized momentum P_x, as

$$\begin{aligned} P_x &= \frac{\partial \mathcal{L}}{\partial \dot{x}} = \psi(x)\dot{x}\,, \\ \text{inverting} \qquad &\Rightarrow \dot{x} = P_x/\psi\,. \end{aligned}$$

Going through the Legendre transform, we get the Hamiltonian $\mathcal{H}$:

$$\begin{aligned} \mathcal{H} &= \dot{x}\,P_x - \mathcal{L}\,, \\ \mathcal{H} &= \frac{1}{2}P_x^2/\psi + \mathbb{P}\,. \end{aligned} \tag{23}$$

The equations of motion for the two-variable system are then,

$$\dot{x} = \frac{\partial \mathcal{H}}{\partial P_x}\,, \quad \dot{P}_x = -\frac{\partial \mathcal{H}}{\partial x}\,. \tag{24}$$

The role of dissipation We shall make a note here about the dissipation which plays a crucial role in the long-term behaviour of a realistic physical system. Realistic numbers in the literature [2] yield the force of dissipation on the k-th oscillator as $\sim \gamma \dot{u}_k$ where $\gamma \sim 10^{-4}$. One could try to insert the averaging ansatz (1) directly into the total dissipation rate $\sum_k -\gamma \dot{u}_k^2$ and compute the dissipation force; however, in our opinion, such approach is inconsistent. A correct way would be to use the ansatz (1) in the Euler-Lagrange equations obtained from the Lagrangian (4) and proceeding with the averaging. Note that this approach, amounting to averaging the equations of motion *after* computing the Euler-Lagrange equation, is quite different – and more complex – than the method presented here, where the averaging is done directly in the Lagrangian *before* computing the Euler-Lagrange equations. While it is possible to proceed using the first method, one would need to be consistent and use the direct averaging of each term in the equations of motion rather than averaging the Lagrangian. We shall not follow this approach here, as it does not allow the canonical formalism developed above.

3.2 Results

To examine the dynamics of this system, rather than solving ODE system (24) directly, we look at the energy landscape. Indeed, $\mathcal{H}$ is conserved in time, as $\frac{d}{dt}(\mathcal{H}) = 0$. Hence, the level sets of $\mathcal{H}$ indicate paths in $(x,\, P_x)$-space through time. An example of such level sets is given in Figure 2. There are periodic orbits appearing in the bottom of the energy wells, seen in dark blue, and escaping trajectories further up the walls, seen in yellow and red. These are the only two types of trajectories appearing as level sets, so the dynamics of this system is rather minimal, and is topologically equivalent to that of a simple pendulum.

The inclusion of defect in the system serves to deform the energy landscape by lowering or raising the boundary between local minima, depending on the sign of the defect. If the defect lowers the

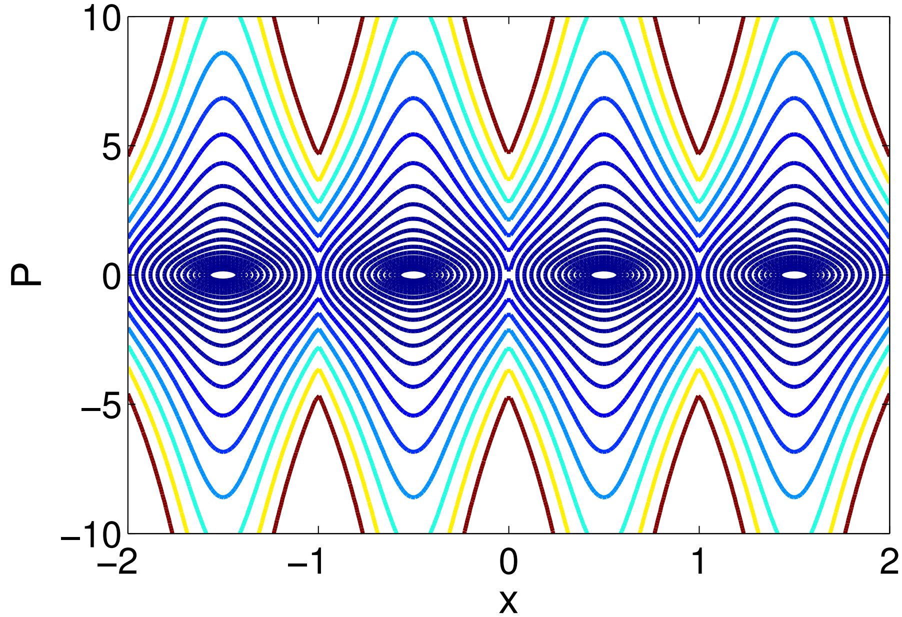

Fig. 2. Level sets, for the two variable system, of $\mathcal{H}$ (23), which is conserved. Trajectories are either oscillatory about a local minimum, or escaping. Defects lower or raise the boundary between minimal energy states, strengthening pinning, or allowing travel between multiple pillars.

parameter, it will permit movement of the ILM between pillars and possible capture into a potential well from an exponentially small measure (as a function of the distance x). Alternatively, the defect that raises the energy values will facilitate an escape from the bounded trajectories of the potential well.

While this simple two-dimensional system does demonstrate some interesting features like traveling ILMs and capture of ILMs, it is too simplistic to accurately describe complex dynamics of ILMs exhibited by physical systems. Most notably, ILMs in experiment and simulation never remain stationary with constant amplitude, nor do they travel at averaged constant speed with constant amplitude. On the contrary, experimentally observed ILMs have finite lifetime, and the amplitude tends to vary with time. Moreover, a general agreement [6] seems to be that it is impossible for an ILM to propagate with a constant speed. Thus, the results of this simplistic model are inconsistent with current knowledge about ILM and an improvement of the model must be sought. Such an improvement is achieved below by allowing the amplitude A to depend on time. This increases the number of variables in the reduced system from two to four and permits much richer behaviour of ILMs, which is closer to the one observed in numerical simulations for the full system and experiments.

4. Four Dimensional Model

4.1 Derivation

The four-dimensional model accounts for change in both the amplitude A of the ILM, as well as its peak position x. Whereas the two variable model was too simple to allow complicated dynamics, our 4D system will be much more realistic.

Kinetic Energy Still working with (1) for the ILM form, but with $x = x(t)$, $A = A(t)$, we have a new expression for the velocity of each pillar:

$$\dot{u}_n = \left(\dot{A}\cos\omega t - A\omega\sin\omega t + \lambda A\,\mathrm{sign}(n-x)\dot{x}\cos\omega t\right)(-1)^n e^{-\lambda|n-x|}\,, \tag{25}$$

$$\Rightarrow\ \dot{u}_n^2 = \frac{e^{-2\lambda|n-x|}}{2}\left(\omega^2A^2 + \dot{A}^2 + A^2\lambda^2\dot{x}^2 + 2A\lambda\mathrm{sign}(n-x)\dot{A}\dot{x}\right)\,, \tag{26}$$

after averaging the time functions. Substituting (26) into $\mathcal{K}$, we get

$$\mathcal{K} = \frac{1}{2}\sum_{-\infty}^{\infty} \dot{u}_n^2 = \frac{E_2}{4\xi_2}\left(\omega^2 A^2 + \dot{A}^2 + A^2\lambda^2\dot{x}^2\right) + A\lambda\dot{A}\dot{x}\frac{1}{2}\sum_{-\infty}^{\infty} e^{-2\lambda|n-x|}\mathrm{sign}(n-x)\,, \tag{27}$$

with the shorthand,

$$E_2 = e^{-2\lambda(n_0+1-x)} + e^{-2\lambda(x-n_0)}\,, \tag{28}$$
$$\tilde{E}_2 = e^{-2\lambda(n_0+1-x)} - e^{-2\lambda(x-n_0)}\,, \tag{29}$$
$$\xi_2 = 1 - e^{-2\lambda}\,. \tag{30}$$

We turn our attention to the the sum in (27). As long as x is not an integer, this expression may be written as

$$\mathbb{E} = \sum_{-\infty}^{\infty} e^{-2\lambda|n-x|}\mathrm{sign}(n-x) = \frac{1}{\xi_2}\left(e^{-2\lambda(n_0+1-x)} - e^{-2\lambda(x-n_0+1)}\right) + \mathrm{sign}(n_0-x)e^{-2\lambda(x-n_0)} \tag{31}$$

$\mathbb{E}$ has a discontinuity at $x = n_0$, when the ILM is centered *at* a pillar; this occurs at a set of measure 0, so we disregard it, and hereafter assume $\mathbb{E} = \tilde{E}_2/\xi_2$. Therefore, we write the final expression for our kinetic energy:

$$\mathbb{K} = \frac{1}{4}\left(\dot{A}^2 + A^2\omega^2 + \lambda^2 A^2\dot{x}^2\right)\frac{E_2}{\xi_2} + \frac{1}{2}A\dot{A}\lambda\dot{x}\mathbb{E} \tag{32}$$
$$= \frac{1}{4}\frac{E_2}{\xi_2}\dot{A}^2 + \frac{\lambda^2 A^2}{4}\frac{E_2}{\xi_2}\dot{x}^2 + \frac{A\lambda}{2}\mathbb{E}\dot{A}\dot{x} + \frac{A^2\omega^2}{4}\frac{E_2}{\xi_2}\,. \tag{33}$$

Potential Energy The potential energy $\mathbb{P}$ for the four dimensional reduced system is the same as $\mathbb{P}$ for the two variable system, as in (8, 19).

Hamiltonian Mechanics We first write the Langrangian

$$\mathcal{L} = \mathbb{K} - \mathbb{P}\,, \quad \text{or} \tag{34}$$
$$\mathcal{L} = \frac{F_1}{2}\dot{A}^2 + A^2\frac{F_2}{2}\dot{x}^2 + AF_3\dot{A}\dot{x} - c_2A^2 - c_4A^4\,, \tag{35}$$

where we have defined

$$F_1 = \frac{E_2}{2\xi_2}\,, \quad F_2 = \frac{\lambda^2 E_2}{2\xi_2}\,, \quad F_3 = \frac{\lambda\mathbb{E}}{2}\,. \tag{36}$$

$$c_2 = -\frac{\omega^2 E_2}{4\xi_2} + \mu_2 + \frac{\alpha_D}{2}e^{-2\lambda|x-K|}\,, \tag{37}$$
$$c_4 = \mu_4\,. \tag{38}$$

Hamilton's Equations allow the introduction of canonical variables (P_x, P_A) that are dual to (x, A) through

$$P_A = \frac{\partial\mathcal{L}}{\partial\dot{A}} = F_1\dot{A} + AF_3\dot{x}\,. \tag{39}$$
$$P_x = \frac{\partial\mathcal{L}}{\partial\dot{x}} = A^2F_2\dot{x} + AF_3\dot{A}\,. \tag{40}$$

Inverting these expressions, *i.e.*, solving for $(\dot{x}, \dot{A})$ in (40,39) and denoting, for simplicity, $\Delta = F_1F_2 - F_3^2$, we obtain

$$\dot{A} = \frac{1}{\Delta}(F_2P_A - A^{-1}F_3P_x)\,, \tag{41}$$
$$\dot{x} = \frac{1}{\Delta}(-A^{-1}F_3P_A + A^{-2}F_1P_x)\,. \tag{42}$$

The determinant Δ is written explicitly as

$$\Delta = F_1 F_2 - F_3^2 = \frac{\lambda^2}{4\xi_2^2}(E_2^2 - \tilde{E}_2^2) = \frac{\lambda^2}{\xi_2^2} e^{-2\lambda} \,. \tag{43}$$

Using the Legendre Transform,

$$\mathcal{H} =< p\,, \dot{q} > -\mathcal{L}(q, \dot{q}), \tag{44}$$

we can now define the Hamiltonian $\mathcal{H}$ as follows,

$$\mathcal{H} =\frac{1}{\Delta}\left(\frac{F_2}{2}P_A^2 + A^{-2}\frac{F_1}{2}P_x^2 - A^{-1}F_3 P_A P_x\right) + c_2 A^2 + c_4 A^4. \tag{45}$$

Armed with $\mathcal{H}$, we can derive the equations of motion for the canonically transformed system. It is interesting to note that the Hamiltonian $\mathcal{H}$ is conserved during the motion, providing a useful check of the numerics; however, because of the four-dimensionality of the system, the conservation of the Hamiltonian alone is not sufficient to derive the solutions, in contrast to two-dimensional system (x, P_x). The canonical equations of motion are:

$$\dot{P}_x = -\frac{\partial \mathcal{H}}{\partial x}\,, \quad \dot{P}_A = -\frac{\partial \mathcal{H}}{\partial A} \tag{46}$$

$$\dot{x} = \frac{\partial \mathcal{H}}{\partial P_x}\,, \quad \dot{A} = \frac{\partial \mathcal{H}}{\partial P_A}\,. \tag{47}$$

More explicitly, we write the canonical equations of motion for (x, A, P_x, P_A) as follows:

$$\dot{P}_x = -\left(\frac{1}{\Delta}\left(\frac{1}{2}\frac{\partial F_2}{\partial x}P_A^2 + \frac{1}{2}\frac{\partial F_1}{\partial x}A^{-2}P_x^2 - \frac{\partial F_3}{\partial x}A^{-1}P_A P_x\right) + A^2\frac{\partial c_2}{\partial x} + A^4\frac{\partial c_4}{\partial x}\right)\,, \tag{48}$$

$$\dot{P}_A = -\left(-\frac{F_1}{\Delta}A^{-3}P_x^2 + \frac{F_3}{\Delta}A^{-2}P_A P_x + 2Ac_2 + 4A^3 c_4\right)\,, \tag{49}$$

$$\dot{x} = \frac{F_1}{\Delta}A^{-2}P_x - \frac{F_3}{\Delta}A^{-1}P_A\,, \tag{50}$$

$$\dot{A} = \frac{F_2}{\Delta}P_A - \frac{F_3}{\Delta}A^{-1}P_x\,. \tag{51}$$

4.2 Results

Initial coding of (48 - 51) resulted in ODE which frequently encountered a run-time singularity due to the attractive fixed point $A = 0$. To allow us to pass near the $A = 0$ singularity, we rescale time from t into τ as $\mathrm{d}t = A^p \mathrm{d}\tau$, where p is the lowest power which removes negative powers from the ODEs; in our case, $p = 3$. Essentially, we are rescaling by values of the variable for which there is a singularity, so that as we approach the 'bad' value, time slows down. After a simulation has concluded, we return to normal time by performing the integration

$$t = \int_0^\infty A^p(\tau)\mathrm{d}\tau\,. \tag{52}$$

In all cases, we could continue the simulation until $\tau = \infty$ (or arbitrarily large), in the case when the solution hits the singularity at $A = 0$, it occurs in finite time $t_0 = \int_0^\infty A^3(\tau)\mathrm{d}\tau$. The solutions are then plotted with $A = A(t)$ and $x = x(t)$, with t computed parametrically from τ using (52).

Figure 3 shows a suite of simulations of (48 - 51) with identical parameters such as starting values of $A(0)$ *etc*, except the initial position of the ILM $x_0 = x(0)$. Ten initial conditions are presented here, with the emphasis of interpretation being on diverging paths that seem initially similar. The ILMs oscillate several times, and wander across the array. The ILMs starting from $x_0 = \{-3, -1, 1, 3\}$ represent those whose initial condition is symmetric with respect to the pillar at which they start. This ILM form is the same as that found in *e.g.* [5], and is known to be a stable ILM. In contrast, those simulations here which start in between pillars, represent the anti-symmetric ILM, and are known to

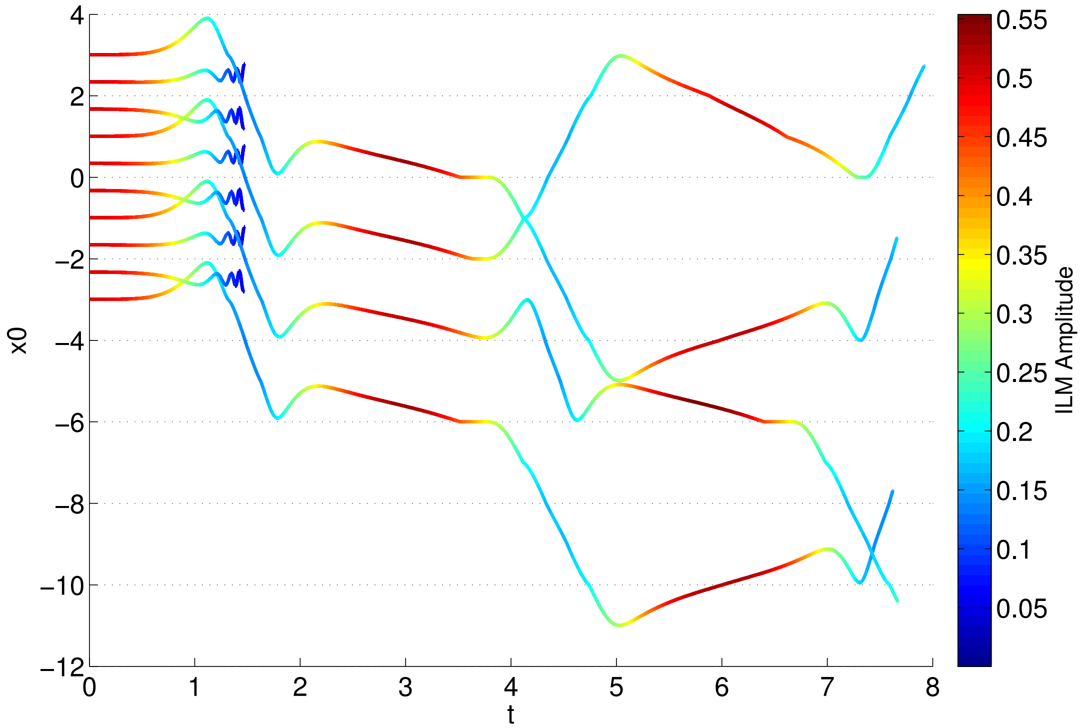

Fig. 3. Four-variable reduced system, simulations of 10 initial conditions. In the absence of defect, the interval of initial conditions between $x_0 = 0$ and $x_0 = 1$ would be perfectly symmetrical; in this plot, a -5% defect at pillar 0 causes a breaking in symmetry. ILMs which have similar initial position, translated by one unit, have similar trajectories at first, before diverging.

be unstable – hence, they die relatively quickly, as the initial amplitude dissipates into momenta until the ILM vanishes.

In Figure 4 is a set of simulations for which the *initial position* is held constant, and instead the two parameters $P_x(t = 0)$ and λ are varied. Increasing the initial value of the dual variable P_x gives the ILM an initial "push", so it tends to move further along the array. In contrast, increasing the value of λ seems to increase the amount of time it takes the ILM to diverge from its initial position. This features mimic the general behaviour observed in full simulations of ILMs, for example, propagation of ILMs through arrays.

Another interesting feature of the model is that we do not get a constant speed motion of ILMs, even in an approximate or average sense. Most motions we have observed consists of almost piecewise short "patches" of almost constant velocities, when ILM moves with one speed, then changes abruptly to another speed *etc.*. Note that there is no analytic solution with $\dot{x}$ =const since the right-hand sides of the equations (48-51) explicitly depends on x, so a solution with constant speed must be thought in approximate sense only. That jittery and complex behaviour of ILMs conforms to current literature [6], but more studies are definitely needed for quantitative comparisons.

5. Conclusions

In this paper, we have demonstrated that a reduction of high-dimensional system of coupled oscillators to low-dimensional system based on the reduced description of ILMs results in an interesting and realistic low-dimensional Hamiltonian system of ODEs. We demonstrated that the minimum number of variables to observe interesting behaviour is four, two being the position and the amplitude of ILM and the other two the corresponding canonical momenta. A question naturally arises whether one needs to increase the complexity to improve the model of ODEs even further. While it is true that increasing the number of variables per ILM description does (probably) add more realistic features, we believe that real progress can be achieved now by keeping the model we have derived for an individual ILM and, at the same time, increasing the number of ILMs. Of particular interest is the

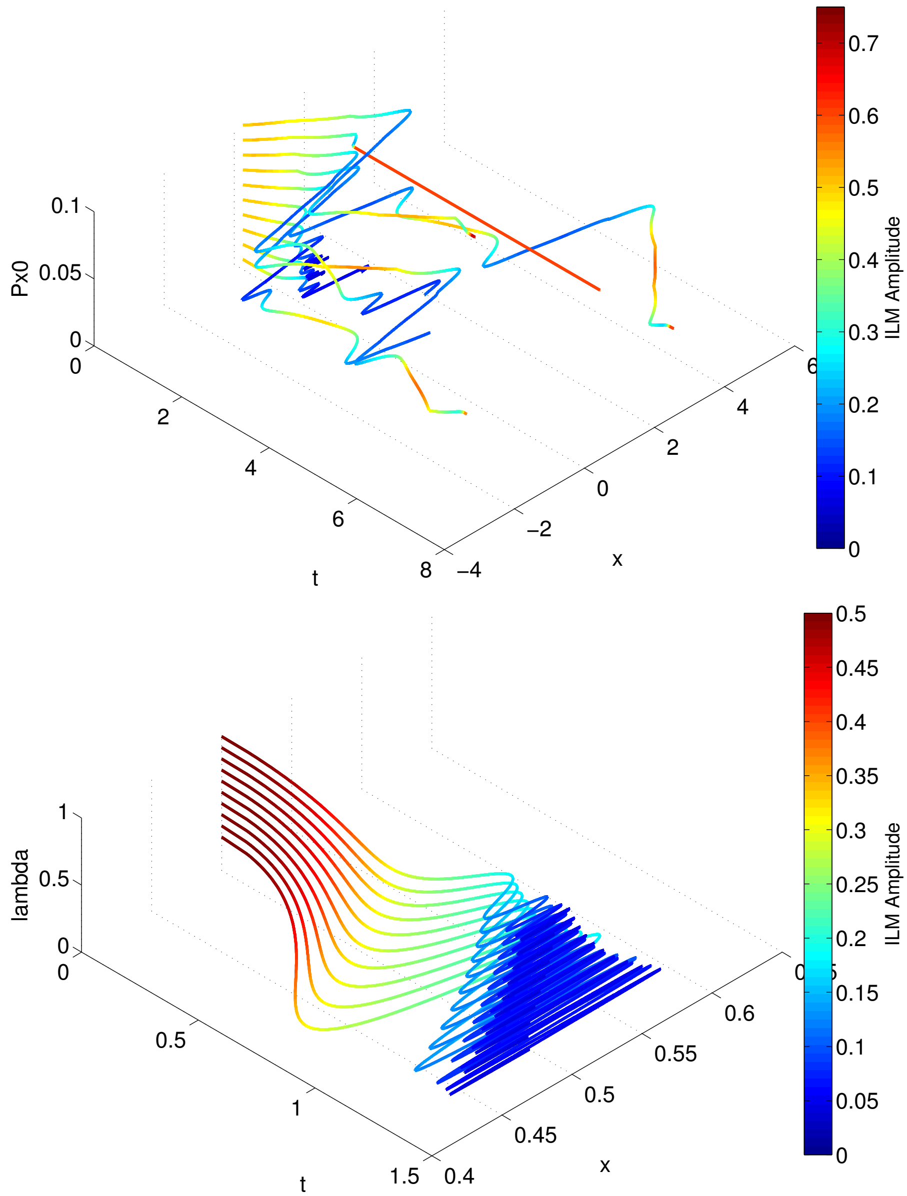

Fig. 4. Four-variable simulations of reduced ILM dynamics. The color of the lines indicates ILM amplitude. Top: In the vertical axis is an exploration of the dual variable in the system, P_x. Each simulation started from the same point on the array, at $x = 0.25$. Increasing the initial value of P_x pushes the ILM in the positive direction on the array. Bottom: Varying the value of parameter λ alters how quickly the ILM diverges from its initial position, with higher values leaving the ILM in place for longer.

influence of defects and appearance of new ILMs. An analytical description of defect's influence can be constructed here, much like the one outlined in the previous section.

We discussed solutions, conservation laws due to the Hamiltonian structure and the application of averaging principle. We believe that this work opens some interesting possibilities for constructing low-dimensional models of ILM motion and the corresponding (almost) analytical description of the influence of defects on ILMs.

Finally, we will briefly say how the ILMs are affected by defects in this model. An analytical description of defect's influence can be constructed here, much like the one outlined in the previous section. Note, however, that we enforce the number of ILMs to be constant, so new ILMs cannot be born out of interactions with defects. It would be interesting to see if one can generalize this model to account for birth of ILMs, for example, by placing several of "ghost" ILMs with very small amplitudes.

One obstacle in the path of multi-ILM description lies in the fact that $A = 0$ is a singularity in equations. Several methods can be derived to deal with that singularity. For example, one can locally use the variable $B = A^{-p}$ for some power $p > 0$ and make a continuum transition through $A = 0$. Unfortunately, this introduces singularities in other equations, so a careful analysis through scaled time must be undertaken. Another option is to introduce a small ad-hoc term in the $\dot{A}$ equation preventing $A(t)$ from reaching the singular point $A = 0$. The right choice of such a term which will not affect the motion away from $A = 0$ is rather tricky and will be undertaken in future work.

Another interesting direction will be to extend the results of this system to two-dimensional oscillations of pillars as described in [2]. We believe that such a system, which must necessarily involve involving six canonical variables (one position x and two amplitudes A and B for out-of-plane and in-plane oscillations, and the corresponding momenta), should provide a consistent low-dimensional description of ILM behaviour.

Acknowledgements

We have benefitted from fruitful discussions with Profs. T. Hikihara, M. Kimura, M. Marconi and M. Sato. This project received support from the Defense Threat Reduction Agency – Joint Science and Technology Office for Chemical and Biological Defense (Grant no. HDTRA1-10-1-007).

References

[1] P. W. Anderson. Absence of diffusion in certain random lattices. *Phys. Rev.*, 109:1492–1505, Mar 1958.

[2] Daniel Brake, Huiwen Xu, Andrew Hollowell, Ganesh Balakrishnan, Chris Hains, Mario Marconi, and Vakhtang Putkaradze. Intrinsic localized modes in two-dimensional vibrations of crystalline pillars and their application for sensing. *Journal of Applied Physics*, 2012.

[3] Valeriy A. Brazhnyi and Boris A. Malomed. Localization and delocalization of two-dimensional discrete solitons pinned to linear and nonlinear defects. *Phys. Rev. E*, 83:016604, 2011.

[4] V. M. Burlakov, S. A. Kiselev, and V. N. Pyrkov. Computer simulation of intrinsic localized modes in one-dimensional and two-dimensional anharmonic lattices. *Phys. Rev. B*, 42(8):4921–4927, 1990.

[5] A.J. Dick, B. Balachandran, and Jr. Mote, C.D. Intrinsic localized modes in microresonator arrays and their relationship to nonlinear vibration modes. *Nonlinear Dynamics*, 54:13–29, 2008.

[6] S. Flach and A. V. Gorbach. Discrete breathers – advances in theory and applications. *Physics Reports*, 467:1–116, 2008.

[7] S. Gutschmidt and O. Gottlieb. Bifurcations and loss of orbital stability in nonlinear viscoelastic beam arrays subject to parametric actuation. *Journal of Sound and Vibration*, 329(18):3835 – 3855, 2010.

[8] Guoxiang Huang, Zhu-Pei Shi, and Zaixin Xu. Assymetric intrinsic localized modes in a homogeneous lattice with cubic and quartic anhamonicity. *Phys. Rev. B*, 47(21), June 1993.

[9] P. G. Kevrekidis, S. V. Dmitriev, S. Takeno, A. R. Bishop, and E. C. Aifantis. Rich example of geometrically induced nonlinearity: From rotobreathers and kinks to moving localized modes and resonant energy transfer. *Phys. Rev. E*, 70(6):066627, Dec 2004.

[10] P. G. Kevrekidis and V. V. Konotop. Bright compact breathers. *Phys. Rev. E*, 65(6):066614, Jun 2002.

[11] P.G. Kevrekidis, A.R. Bishop, and K. Ø. Rasmussen. Twisted localized modes. *Phys. Rev. E*, 63(3), 2001.

[12] M. Kimura and T. Hikihara. Capture and release of traveling intrinsic localized mode in coupled cantilever array. *Chaos*, 19(1):13138, 2009.

[13] Masayuki Kimura and Takashi Hikihara. Coupled cantilever array with tunable on-site nonlinearity and observation of localized oscillations. *Phys. Lett. A*, 373(14):1257 – 1260, 2009.

[14] NOLTA. *Simplified models for Intrinsic Localized Mode dynamics*, October 2012.

[15] J. B. Page. Asymptotic solutions for localized vibrational modes in strongly anharmonic periodic systems. *Phys. Rev. B*, 41(11):7835–7838, Apr 1990.

[16] S. Ramakrishnan and B. Balachandran. Intrinsic localized modes in micro-scale oscillator arrays subjected to deterministic excitation and white noise. In B. Dattaguru, S. Gopalakrishnan, and V. K. Aatre, editors, *IUTAM Symposium on Multi-Functional Material Structures and Systems*, volume 19 of *IUTAM Bookseries (closed)*, pages 325–334. Springer Netherlands, 2010.

[17] M. Sato, B. E. Hubbard, L. Q. English, A. J. Sievers, B. Ilic, D. A. Czaplewski, and H. G. Craighead. Study of intrinsic localized vibrational modes in micromechanical oscillator arrays. *Chaos*, 13(2):702, May 2003.

[18] M. Sato, B. E. Hubbard, and A. J. Sievers. Colloquium: Nonlinear energy localization and its manipulation in micromechanical oscillator arrays. *Rev. Mod. Phys.*, 78(1):137–157, Jan 2006.

[19] M. Sato, B. E. Hubbard, A. J. Sievers, B. Ilic, D. A. Czaplewski, and H. G. Craighead. Observation of locked intrinsic localized vibrational modes in a micromechanical oscillator array. *Phys. Rev. Lett.*, 90(4):044102, Jan 2003.

[20] M. Sato and A. J. Sievers. Direct observation of the discrete character of intrinsic localized modes in an antiferromagnet. *Nature*, 432(7016):486–488, 11 2004.

[21] M. Sato and A. J. Sievers. Visualizing intrinsic localized modes with a nonlinear micromechanical array. *Low Temp. Phys.*, 34(7):543–548, 2008.

[22] A. J. Sievers and S. Takeno. Intrinsic localized modes in anharmonic crystals. *Phys. Rev. Lett.*, 61(8):970–973, Aug 1988.